J|A|C|S
ARTICLES
Published on Web 12/04/2002

NMR Determination of the Conformation of a Trimethylene Interstrand Cross-Link in an Oligodeoxynucleotide Duplex Containing a 5′-d(GpC) Motif

Patricia A. Dooley,[§] Mingzhou Zhang,[‡] Gregory A. Korbel, Lubomir V. Nechev,[†] Constance M. Harris, Michael P. Stone, and Thomas M. Harris*

Contribution from the Department of Chemistry and Center in Molecular Toxicology, Vanderbilt University, Nashville, Tennessee 37235

Received June 4, 2002

Abstract: Malondialdehyde interstrand cross-links in DNA show strong preference for 5′-d(CpG) sequences. The cross-links are unstable and a trimethylene cross-link has been used as a surrogate for structural studies. A previous structural study of the 5′-d(CpG) cross-link in the sequence 5′-d(AGGCG*CCT), where G* is the modified nucleotide, by NMR spectroscopy and molecular dynamics using a simulated annealing protocol showed the guanine residues and the tether lay approximately in a plane such that the trimethylene tether and probably the malondialdehyde tether, as well, could be accommodated without major disruptions of duplex structure [Dooley et al. *J. Am Chem. Soc.* **2001**, *123*, 1730−1739]. The trimethylene cross-link has now been studied in a GpC motif using the reverse sequence. The structure lacks the planarity seen with the 5′-d(CpG) sequence and is skewed about the trimethylene cross-link. Melting studies indicate that the trimethylene cross-link is thermodynamically less stable in the GpC motif than in the 5-d(CpG). Furthermore, lack of planarity of the GpC cross-link precludes making an isosteric replacement of the trimethylene tether by malondialdehyde. A similar argument can be used to explain the 5′-d(CpG) preference for interchain cross-linking by acrolein.

Introduction

DNA cross-linking agents frequently exhibit sequence specificity for target nucleotides. The sequence preference is a function of structural constraints in the DNA duplex. Kinetic considerations determine sequence selectivity with agents that form cross-links by mechanisms that are effectively irreversible. For example, the nitrogen mustards produce interchain cross-links in DNA by alkylation of N7 of guanines selectively in 5′-d(GNC) sequences.[1,2] Diepoxybutane[3] and 2,5-bis(1-aziridinyl)-1,4-benzoquinone also react at guanine N7 positions and show the same sequence preferences.[4] Reductively activated mitomycin C forms interchain cross-links between exocyclic amino groups of guanine residues in 5′-d(CpG) sequences.[5] The same sequence specificity is seen for interchain cross-linking by nitrous acid,[6] and pyrrole-derived bis-electrophiles.[7] The sequence specificities in these cases are determined by energetics of transition states not the stabilities of the ultimate products.

With bis-electrophiles that react in a reversible fashion, sequence preferences will be thermodynamically based. An example of this type of cross-linking agent is malondialdehyde (MDA). MDA reacts with DNA to generate simple or cyclic adducts of adenine, cytosine, and particularly guanine (Scheme 1). In addition, there is evidence that DNA−MDA interstrand cross-links are formed and may, in vivo, be the key premutagenic lesions from which mutations arise during repair processes.[8] Niedernhofer found that MDA−DNA cross-links formed preferentially between guanines in a 5′-d(CpG) (hereafter designated as CpG), sequence context.[9] In a screen for sequence specificity of DNA interstrand cross-links, 12 combinations of nucleoside pairs in the center of 18-base-pair oligonucleotide duplexes were synthesized and treated with MDA. Significant interchain cross-linking was seen in the only oligonucleotide having a CpG sequence, suggesting the formation of an interstrand G−G cross-link. The cross-link is unstable, readily reverting to the mono adduct and has, thus far, eluded structural characterization. On the basis of the known chemistry of MDA adducts with nucleosides, it is assumed that the cross-linked species involves the exocyclic amino groups of the guanines.

* Corresponding author. Telephone: (615) 322-2649. Fax: (615) 322-7591. E-mail: harristm@toxicology.mc.vanderbilt.edu.
[§] Current Address: Department of Chemistry, United States Military Academy, West Point, NY 10996.
[‡] Current Address: Neurocrine Biosciences, San Diego, CA 92121.
[†] Current Address: Transgenomic, Inc., Boulder, CO 80301.

(1) Millard, J. T.; Raucher, S.; Hopkins, P. B. *J. Am. Chem. Soc.* **1990**, *112*, 2459−2460.
(2) Rink, S. M.; Solomon, M. S.; Taylor, M. J.; Rajur, S. B.; McLaughlin, L. W.; Hopkins, P. B. *J. Am. Chem. Soc.* **1993**, *115*, 2551−2557.
(3) Millard, J. T.; White, M. M. *Biochemistry* **1993**, *32*, 2120−2124.
(4) Alley, S. C.; Hopkins, P. B. *Chem. Res. Toxicol.* **1994**, *7*(5), 666−72.
(5) Millard, J. T.; Weidner, M. F.; Kirchner, J. J.; Ribeiro, S.; Hopkins, P. B. *Nucleic Acids Res.* **1991**, *19*, 1885−1891.
(6) Kirchner, J. J.; Hopkins, P. B. *J. Am. Chem. Soc.* **1991**, *113*, 4681−4682.
(7) Woo, J.; Sigurdsson, S. T.; Hopkins, P. B. *J. Am. Chem. Soc.* **1993**, *115*, 3407−3415.
(8) Mukai, F. H.; Goldstein, B. D. *Science* **1976**, *191*, 868−869.
(9) Niedernhofer, L. J. Ph.D. Thesis, Vanderbilt University, 1996.

10.1021/ja0207798 CCC: $25.00

Scheme 1

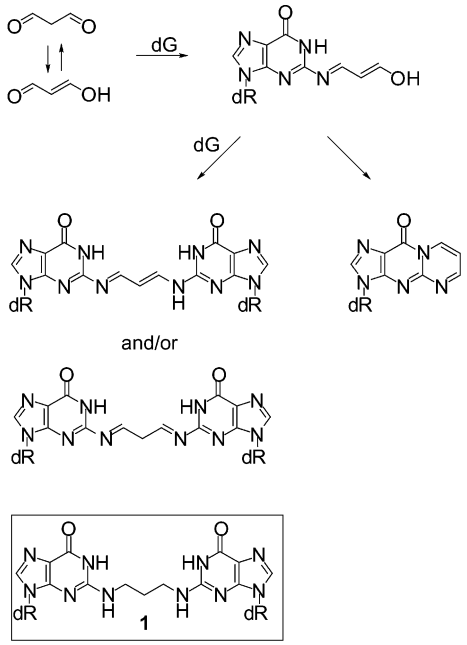

No synthetic strategy has been devised to prepare DNA duplexes containing this cross-link. Consequently, it has not been possible to carry out structural studies on the MDA cross-link to elucidate the basis for the CpG cross-linking preference. In lieu of having DNA containing the actual MDA interstrand cross-link, we recently examined saturated analogue **1**, having a trimethylene cross-link between exocyclic amino groups of guanine, in a CpG sequence context and determined the three-dimensional structure by NMR spectroscopy.[10] The study revealed that the two guanines and the trimethylene linkage all lie in a single plane. An MDA cross-link having four trigonal atoms in the tether could readily be accommodated by this structure. However, the study does not reveal why cross-linking occurs in CpG sequences in preference to 5′-d(GpC). To probe that question, we have now examined the structure of a duplex containing the trimethylene cross-link in a GpC context.

Experimental Section

Synthesis and Purification of Cross-Link 2. Cross-linked oligonucleotide **2** (Scheme 2) was prepared by reaction of diaminopropane with a halopurine-containing 8-mer d(TCCXCGGA), where X = 2-fluoro-O^6-(trimethylsilylethyl)-2′-deoxyinosine, to form monoadducted 8-mer. Reaction with additional halopurine-containing 8-mer yielded cross-link **2**. Details of the synthesis and purification are supplied in the Supporting Information.

NMR Spectra. The concentration of **2** was determined assuming an extinction coefficient of 4.9×10^4 M^{-1} cm^{-1}.[11] All samples were dissolved in 10 mM sodium phosphate buffer containing 0.1 M NaCl and 50 mM EDTA (pH 7.1). For observation of nonexchangeable resonances, samples were lyophilized three times from 99.96% D_2O and finally dissolved in 0.6 mL of 99.996% D_2O, giving a 2 mM concentration of the duplex. For assignments of water-exchangeable protons, the samples were dissolved in a 9:1 H_2O/D_2O buffer of the same composition as above. Spectra were referenced to an internal standard of TSP. Spectra were recorded at a ^1H frequency of 500.13 MHz.

Scheme 2

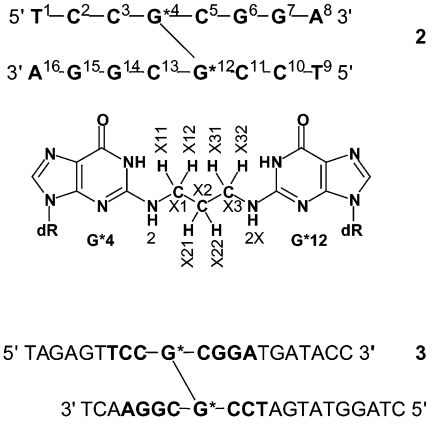

Structural analysis was carried out by methodology in routine use for oligonucleotides. Details of spectral acquisition and analysis are provided in the Supporting Information. Analysis of signals of the trimethylene chain presented special problems. Classical A- and B-DNA were used as the reference structures.[12] The initial models were constructed in INSIGHT II (Biosym Technologies, San Diego, CA) by bonding a propyl group to N^2 of the guanine residue in one strand with the correct orientation and partial charges.[13] Partial charges on the propyl group were obtained from those assigned to propane from the CHARMM force field.[14] The structures were energy-minimized for 100 iterations by the conjugate gradient method to give a monoadducted structure. The creation of the starting structures was completed using X-PLOR 3.1[15] in which the free end of the propyl group was connected to N^2 of the guanine residue in the other strand with the appropriate orientation. Starting structures IniA and IniB were produced upon potential energy-minimization of the cross-linked model compounds using X-PLOR.

Melting and Bending Studies. Melting studies of cross-linked oligonucleotide **2** were carried out as described previously.[10] For bending studies, cross-linked oligonucleotide **3** was synthesized containing the 8-mer sequence of **2**. Bending studies were performed with **3** using the gel mobility shift assay introduced by Koo and Crothers.[16,17] Experimental details are provided in the Supporting Information.

Results

Melting Studies. The UV melting curves of the cross-linked oligodeoxynucleotide 5′-d(TCCG*CGGA)$_2$ and the unmodified duplex of the same sequence are shown in Figure 1A. The melting temperature of the unmodified duplex was 62 ± 1 °C, compared to 52 ± 1 °C for the cross-linked duplex. A thermal melting study in which the imino protons were monitored by one-dimensional (1-D) NMR spectroscopy at 5° increments from 5 to 45 °C was conducted, and the melting profile is shown in Figure 1B. The collapse of the G7 imino proton showed the terminal base-pairs had melted by 25 °C, followed at 35 °C by the next internal base-pair, G6·C11. The melting of the cross-linking G*4 imino proton showed the duplex had unwound by 40 °C.

(10) Dooley, P. A.; Tsarouhtsis, D.; Korbel, G. A.; Nechev, L. V.; Shearer, J.; Zegar, I. S.; Harris, C. M.; Stone, M. P.; Harris, T. M. *J. Am. Chem. Soc.* **2001**, *123*, 1730−1739.
(11) Borer, P. N. *Handbook of Biochemistry and Molecular Biology*, 1st ed.; CRC Press: Cleveland, 1975.
(12) Arnott, S.; Hukins, D. W. L. *Biochem. Biophys. Res. Comm.* **1972**, *47*, 1504−1509.
(13) Hingerty, B. E.; Figueroa, S.; Hayden, T. L.; Broyde, S. *Biopolymers* **1989**, *28*, 1195−1222.
(14) Brooks, B. R.; Bruccoleri, R. E.; Olafson, B. D.; States, D. J.; Swaminathan, S.; Karplus, M. *J. Comput. Chem.* **1983**, *4*, 187−217.
(15) Brunger, A. T. *X-Plor*: version 3.1: A System for X-ray Cry*stallography and NMR*; Yale University Press: New Haven, 1992.
(16) Koo, H. S.; Crothers, D. M. *Proc. Natl. Acad. Sci. U.S.A* **1988**, *85*, 1763−1767.
(17) Koo, H. S.; Wu, H. M.; Crothers, D. M. *Nature* **1986**, *320*, 501−506.

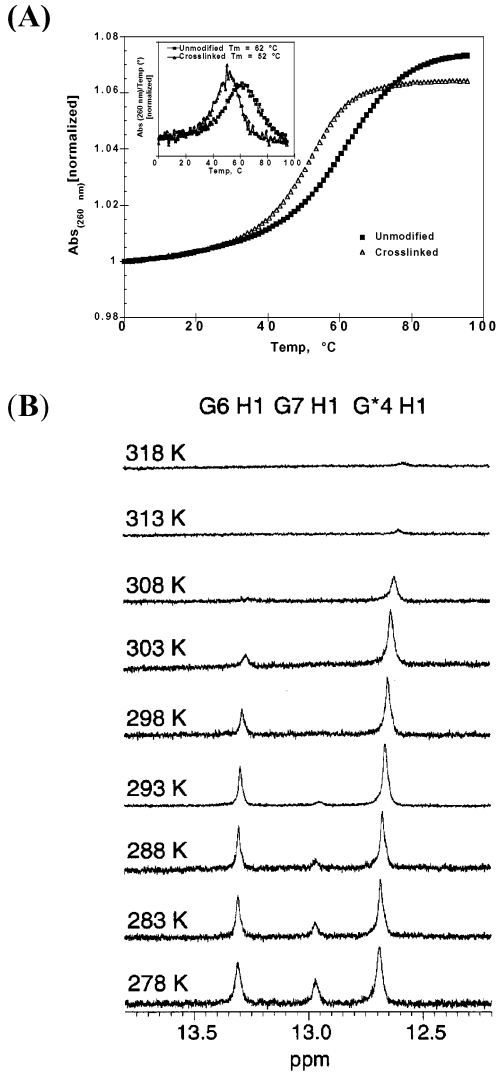

Figure 1. (A) Melting curves of the unmodified and trimethylene cross-link oligodeoxynucleotides 5′-d(TCCG*CGGA)$_2$ measured in 10 mM sodium phosphate buffer (pH 7.1) containing 1.0 M NaCl and 0.05 mM EDTA. The absorbance at which the hyperchromicity was monitored was 260 nm. (Insert) First derivative of the melting curves, indicating $T_m = 62$ °C for the unmodified duplex; 52 °C for the cross-link. (B) Expanded imino ^{1}H region of the trimethylene cross-link oligodeoxynucleotide 5′-d(TCCG*CGGA)$_2$ in 90% H_2O−10% D_2O at 5 °C increments. All of the guanine imino protons, including G*4 (G*12) of the cross-link tether, exchanged with the solvent at the measured temperatures.

In our earlier study of the melting behavior of the 8-mer duplex 5′-d(AGGCG*CCT)$_2$ where the cross-link is in a CpG motif the unmodified duplex showed a melting temperature of 60 ± 1 °C while the presence of the tether produced a large increase in melting temperature.[10] The highest temperature examined, 85 °C, was still significantly below the melting transition. The difference in melting temperatures for the two cross-linked oligonucleotides can be estimated to be in excess of 60 °C.

Bending Studies. For the determination of bending deformations in DNA duplexes, the method of Koo and Crothers[16,17] employing electrophoretic mobilities is more reliable than NMR spectroscopy. A cross-linked 21-mer (**3**) containing the 8-mer cross-link sequence (boldface) was phosphorylated on its 5′ terminus, then ligated to form multimers. In a companion experiment the unmodified 21-mer duplex was treated in the same manner. Electrophoresis of the ligation products was carried out under nondenaturing conditions (8% polyacrylamide). No significant difference in mobilities was observed between the two samples, indicating that no significant bending was induced by the cross-link. Details of this study are provided in the Supporting Information.

^{1}H Resonance Assignments. (a) Nonexchangeable Protons. Similar to the oligomer containing the trimethylene cross-link in the CpG sequence, a single set of resonances in the 1-D ^{1}H spectrum and a single set of cross-peaks in the NOESY spectrum of 5′-d(TCCG*CGGA)$_2$ were observed, that is, symmetry in the self-complementary deoxyoligonucleotide was also retained in the adducted duplex of reverse sequence. Sequential assignments of nonexchangeable protons were determined at 25 °C in the standard manner[18,19] and compared with the assignments of nonexchangeable protons in the unmodified duplex, 5′-d(TCCGCGGA)$_2$. The sequential assignment of internucleotide base aromatic protons and sugar H1′ protons showed continuous connectivity throughout the length of the oligodeoxynucleotide. Overlap of the resonance cross-peaks between T1H6−C2H5 and C5H6−G*4H1′ in the D_2O NOESY spectrum at 25 °C was resolved in the H_2O NOESY spectrum at 5 °C, confirming the internucleotide connectivity, although the C5H6−G*4H1′ cross-peak was weak. A minor overlap problem occurred for G*4 and C2 H1′ resonances, but this did not prevent assignment of other proton resonances for these nucleotides, most of which were well resolved. The assignments of the H2′ and H2″ sugar protons were made on the basis of NOEs and DQF-COSY splitting patterns with the respective H1′ protons. Assuming the oligonucleotide conformed to a B-like DNA structure, the H1′−H2″ distances would be shorter than the H1′−H2′ distances, so that the stronger cross-peaks were assigned to the H2″ resonances. The splitting patterns between H1′−H2′ and H1′−H2″ in the DQF-COSY corroborated the assignments of H2′ and H2″ protons. Both C5 and G6 residues had nearly isochronous H2′ and H2″ resonances, making unambiguous assignments impossible. The relative upfield−downfield relationship of H2′−H2″ resonances was reversed for both G*4 and A8 residues; in both cases, the H2′ resonances were downfield from the H2″ resonances. In the case of the 3′-terminal residue A8, this reversal is not unexpected; for the G*4 residue, however, the reversal may signify nonhelicity.[20]

(b) Exchangeable Protons. Assignments of the imino and amino protons for the unmodified and cross-linked deoxyoligonucleotides were made from NOESY spectra measured at 5 °C in 90% H_2O.[21] Cross-peaks between cytosine H5 protons and non-hydrogen-bonded cytosine amino protons (NH_{2a}) enabled the assignment of the latter. The assignment of the hydrogen-bonded cytosine amino protons (NH_{2b}) was then made on the basis of cross-peaks to NH_{2a} protons. Cross-peaks between guanine imino protons and both NH_{2a} and NH_{2b} protons of base-paired cytosine nucleotides confirmed the imino proton assignments made in the thermal melting study. Assignments based on the observed order of imino proton melting, expected

(18) Hare, D. R.; Wemmer, D. E.; Chou, S. H.; Drobny, G.; Reid, B. R. *J. Mol. Biol.* **1983**, *171*, 319−336.
(19) Feigon, J.; Leupin, W.; Denny, W. A.; Kearns, D. R. *Biochemistry* **1983**, *22*, 5943−5951.
(20) Blommers, M. J. J.; Van De Ven, F. J. M.; Van Der Marel, G. A.; Van Boom, J. H.; Hilbers, C. W. *Eur. J. Biochem.* **1991**, *201*, 33−51.
(21) Boelens, R.; Scheek, R. M.; Dijkstra, K.; Kaptein, R. *J. Magn. Reson.* **1985**, *62*, 378−386.

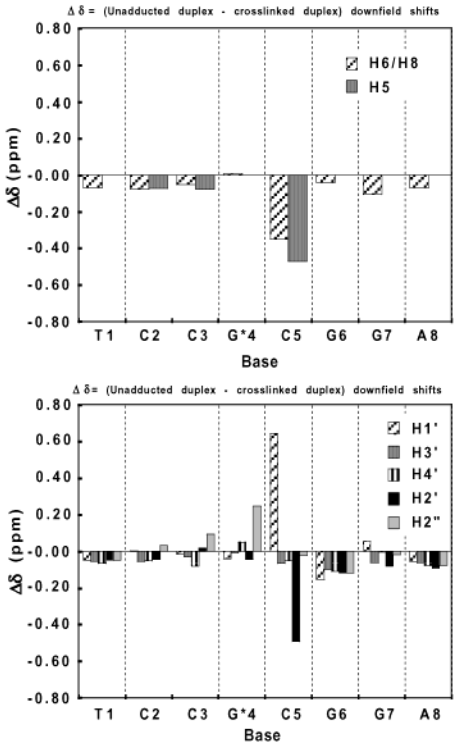

Figure 2. Chemical shift differences of nonexchangeable aromatic and deoxyribose protons of the unadducted and cross-linked oligodeoxynucleotides. (A) Aromatic H5, H6, and H8 protons. (B) Sugar protons. The majority of the structural perturbations are observed in C5, the adjacent and base-pairing residue of the adducted G*4.

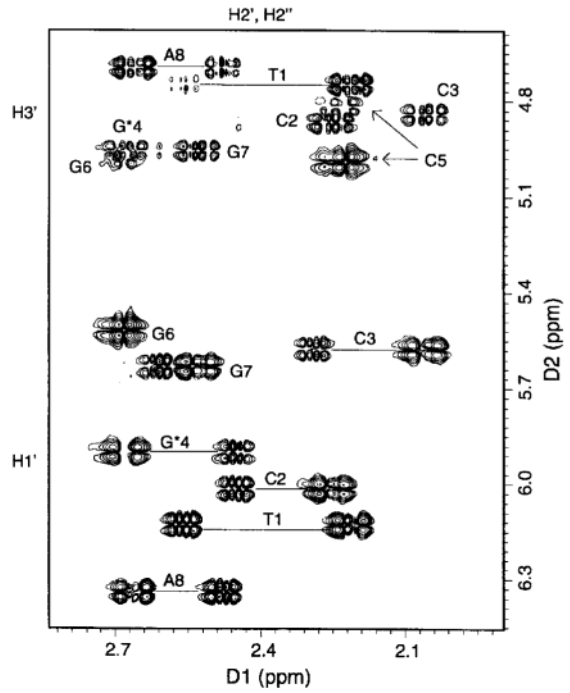

Figure 3. Expanded deoxyribose H1′−H2″, H1′−H2′, and H1′−H3′ regions of the ^{31}P-decoupled DQF-COSY spectrum of the cross-linked oligodeoxynucleotide 5′-d(TCCG*CGGA)$_2$. The assignment of the resonance for each residue is shown adjacent to the cross-peaks.

to be from terminal to internal guanine residues, coincided with the imino proton assignments obtained from the NOESY experiment.

The chemical shifts of the sugar and base protons of the cross-linked oligodeoxynucleotide 5′-d(TCCG*CGGA)$_2$ are shown in Table S1 (Supporting Information). The carbon atom bonded to G*4 N2 is identified as C1, and the central methylene group carbon atom is identified as C2.

(c) Chemical Shift Perturbations. A comparison of the chemical shifts of the unmodified and cross-linked duplexes is shown in Figure 2. Notable spectral features of the cross-linked oligodeoxynucleotide, relative to the unmodified DNA, were the upfield shifts of the H1′ of nucleotide C5 and H2″ of G*4 and the downfield shifts of H2′, H5, and H6 of nucleotide C5. The other residues showed smaller, varying shifts relative to the unmodified oligomer attributable to temperature differences.

No resonances were observed between the terminal base pairs T1·A16 (A8·T9) due to exchange broadening. NOE connectivity was observed from the imino protons of base pairs C2·G15 to C3·G14 to G*4·C13. Since the duplex is self-complementary and only one set of cross-peaks is seen, the connectivity can be extended through base pairs C*5·G12 to G6·C11 to G7·C10. Further evidence for Watson−Crick base-pairing was seen in the cross-peaks between the guanine imino protons and the amino protons of the base-pairing cytosine residues.

The exocyclic amino proton of G*4 in the cross-linked oligomer was nearly isochronous with C2 NH_{2b}. At 8.46 ppm, this resonance was further downfield than broadened resonances of exocyclic amino protons of the other guanine nucleotides (∼6.8 ppm), and it did not melt at increased temperatures, as shown in the 1-D NMR spectra of the thermal melting study. Further, the G*4 exocyclic amino resonance showed a strong cross-peak to the G*4 imino proton and the trimethylene cross-link protons, as described below.

(d) Trimethylene Cross-Link Protons. The resonances arising from the six protons of the trimethylene cross-link were well-resolved from any sugar proton resonances. Only three sets of resonances appeared, further indicating a symmetric conformation about the trimethylene cross-link. The furthest upfield resonance (1.9 ppm) was tentatively assigned to the central methylene protons, and the other resonances (3.7 and 3.1 ppm) to the protons on the methylene carbon atom adjacent to the exocyclic amino group of G*4(G*12). In the NOESY spectrum measured in 90% H_2O, cross-peaks were found between each of the trimethylene protons and both the imino proton and the exocyclic amino proton of G*4. No other cross-peaks to the protons of the trimethylene cross-link were observed anywhere else in the spectrum, a feature which dictated the acceptability of structures which emerged from simulated annealing molecular dynamics, to be discussed later. The intensities of the cross-peaks between the central methylene group protons (1.9 ppm) and each of the vicinal methylene protons adjacent to the exocyclic amino group of G*4 (3.1 and 3.8 ppm) were almost identical.

DQF-COSY Coupling Constants and Pseudorotation Angle. Analysis of the deoxyribose ring through a ^{31}P-decoupled DQF-COSY experiment provided structural data about the phosphate-sugar backbone of the oligodeoxynucleotide 5′-d(TCCG*CGGA)$_2$. Figures 3 and 4 show the regions of the ^{31}P-decoupled DQF-COSY spectrum from which the pseudorotation angle was estimated.

The relationships between pseudorotation angle (P) and coupling constants for H3′−H4′ and H2″−H3′ were used to

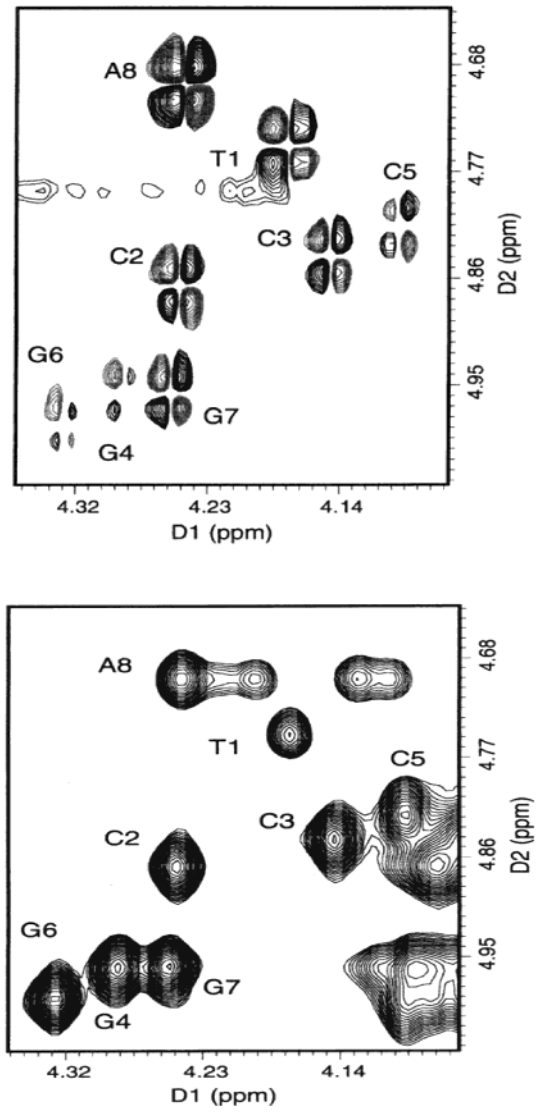

Figure 4. Expanded deoxyribose H3′−H4′ region of the ^{31}P-decoupled DQF-COSY (top) and 350 ms mixing time NOESY (bottom) spectra of the cross-linked oligodeoxynucleotide 5′-d(TCCG*CGGA)$_2$. Nucleotide assignments are indicated near the residues' cross-peaks.

estimate the values of P for the residues of the GpC cross-link.[22] The presence of a cross-peak between H2″ and H3′, as in the case of residues T1 and A8, was indicative of a large coupling constant (Figure 3). Large values for $J_{H2''-H3'}$ correlated to pseudorotation angles between 72 and 100°, the O4′-endo conformational range. Conversely, a weak coupling constant for $J_{H2''-H3'}$ was assigned to the interior deoxyribose rings, since no cross-peaks between H2″ and H3′ were visible. Small $J_{H2''-H3'}$ coupling constants correlated with pseudorotation angle values within the range of 120−162° and with short distances between these protons, typical of C2′-endo conformation.

The relative strengths of the cross-peaks between H3′ and H4′ confirmed the tentative assignments of pseudorotation angles. The cross-peaks in this region of the spectrum (Figure 4) for residues T1 and A8 were significantly stronger than those of the other residues. Residues G4, C5, and G6 showed the weakest of cross-peaks, while C2, C3, and G7 were of medium intensity. Stronger cross-peaks implied a larger dihedral angle between H3′ and H4′, and thus a longer distance between atoms. Weaker cross-peaks were associated with smaller dihedral angles and shorter H3′−H4′ interproton distances, again typical of C2′-endo conformation. The side-by-side comparison of NOESY and DQF-COSY cross-peaks confirmed the expectation that weaker DQF-COSY resonances correlated with stronger NOE intensities, while stronger DQF-COSY cross-peaks correlated with weaker NOE cross-peaks. Therefore, strong DQF-COSY cross-peaks for T1 and A8 led to the assignment of large $J_{H3'-H4'}$ values, which corresponded to the same pseudorotation angle range: 72−100°. A smaller value of $J_{H3'-H4'}$ was assigned to the residues C2, C3, and G7 with medium DQF-COSY cross-peaks. Taking both $J_{H2''-H3'}$ and $J_{H3'-H4'}$ into account, the pseudorotation angle range for these residues was assigned: 120−160°. The smallest value of $J_{H3'-H4'}$ was assigned to the weakest DQF-COSY cross-peaks for residues G4, C5, and G6, and considering the values of $J_{H2''-H3'}$, a tighter range of 140−160° was assigned to the pseudorotation angle.

The splitting patterns of the cross-peaks between H1′ and H2′/H2″ and between H3′ and H2′/H2″, both above and below the diagonal, were then compared to graphical splitting patterns and literature values for pseudorotation angles. Good correlation was observed between published values and those estimated above, so that the δ torsional angle of the backbone sugar residues was determined.

Using 35° for the pucker amplitude Θ_m, a value within a range observed for most A- and B-DNA type sugars, and the ranges of pseudorotation angle P estimated above, the range for dihedral backbone angle δ (O5′−C5′−C4′−C3′)[23] was calculated according to the following equation:[24]

$$\delta = 120.6 + 1.1\,\Theta_m \cos(P + 145.2)$$

The δ angle values which appear in Table S2 (Supporting Information) were used in restrained molecular dynamics calculations, to be described below.

Conformation of the Trimethylene Tether. In the absence of NOE restraints between any of the six protons of the trimethylene tether and the nonexchangeable protons of the sugars and bases, determination of the configuration of the three-carbon tether was absolutely critical to elucidating the structure of the oligomer. The basis for establishing a conformation described as helical was derived from both NOE intensity and DQF-COSY fine splitting pattern analyses and is described here.

Symmetry of the Tether. The observation of a single set of resonances, both in 1- and 2-D spectra, indicated the shape assumed by the tether was symmetrical and that the configuration of the DNA was symmetrical.

Intensities of Tether Cross-Peaks. Similar to the cross-link in the CpG sequence, the intensities of the cross-peaks between protons of the cross-link were greater than intensities of comparable geminal and vicinal protons on sugar moieties elsewhere in the DNA. For example, at each of the three NOESY mixing times, the geminal α-methylene (Figure 5, HX1 and HX2) cross-peak intensities were greater than the intensities of geminal H2′−H2″ cross-peaks for residues T1, C2, and C3.

(22) Schweitzer, B. I.; Mikita, T.; Kellogg, G. W.; Gardner, K. H.; Beardsley, G. P. *Biochemistry* **1994**, *33*, 11460−11475.

(23) Saenger, W. *Principles of Nucleic Acid Structure;* Springer-Verlag: New York, 1984.

(24) van Wijk, J.; Huckriede, B. D.; Ippel, J. H.; Altona, C. *Methods Enzymol.* **1992**, *211*, 286−306.

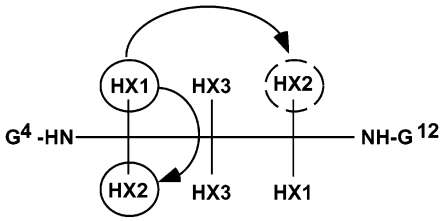

Figure 5. Diagram of geminal cross-link methylene protons. Overlapping resonances between HX1−HX2 (solid circle) and HX1−HX2 (broken circle) contributed to intensity of the cross-peak between HX1 and HX2, observed to be larger than geminal protons of sugar residues in the oligodeoxynucleotide 5′-d(TCCG*CGGA)$_2$.

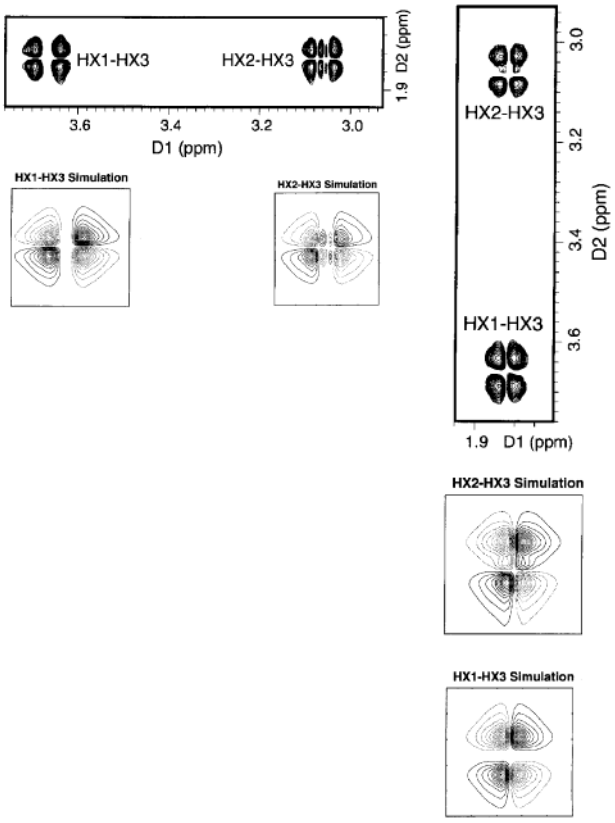

Figure 6. Expanded regions of the ^{31}P-decoupled DQF-COSY showing cross-peaks between vicinal protons HX1 (∼3.7 ppm)−HX3 (∼1.8 ppm) and HX2 (∼3.1 ppm)−HX3 (1.8 ppm), above (horizontal panel) and below (vertical panel) the diagonal. Simulations of the cross-peaks between vicinal protons HX1−HX3 and HX2−HX3 above (left, boxes side by side) and below (right, boxes top and bottom) the diagonal.

The higher intensity of the geminal α-methylene cross-link protons was accounted for by taking into consideration the contribution of overlapping cross-peaks between resonances indicated in Figure 5. The resonances for HX2 near G4 and HX2 near G12 were isochronous, but the protons were at different distances from HX1. The cross-peak contained the overlapping signals of the geminal HX1−HX2 resonance and HX1-distal HX2 resonance, and was consequently of higher intensity than a geminal H2′−H2″ cross-peak.

Similarly, the intensities of cross-peaks between vicinal protons (HX1−HX3 and HX2−HX3) in the trimethylene cross-peak were higher than intensities between vicinal proton cross-peaks (H1′−H2′ and H1′−H2″, respectively) of sugar residues C3, G4, and G7 in the oligodeoxynucleotide. However, the cross-peak intensities between protons depicted in Figure 5 as HX1−HX3 and HX2−HX3 were not identical, whereas the

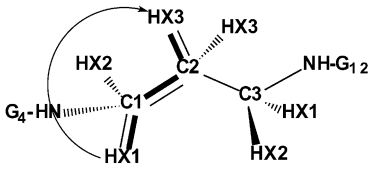

Figure 7. Representation of the trimethylene tether model. Heavy black lines define the dihedral angle initially modeled in INSIGHT II as 90°.

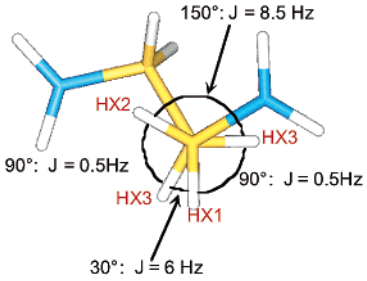

Figure 8. Symmetrical structure of the trimethylene tether in a helical shape. Dihedral angles between methylene protons on adjacent carbons were 30°, 90°, and 150°.

intensities were identical in the CpG sequence. The trimethylene tether in the CpG sequence was, therefore, planar and limited to either a planar W or U conformation. These shapes were excluded from consideration for the GpC sequence because the experimental evidence supported a conformation in which the distances between vicinal protons differed from each other. To find a tether conformation which possessed dyad symmetry and accommodated unequal vicinal proton distances, the fine splitting patterns of the DQF-COSY were examined.

DQF-COSY Fine Splitting Patterns and Simulations. Shown in Figure 6 are the cross-peaks between vicinal protons of the trimethylene cross-link. A simulation of each respective cross-peak is also shown in Figure 6. The noteworthy feature of the cross-peak between HX1−HX3 was the absence of any multiplet component peaks.

Multiplet component peaks were present in the HX2−HX3 cross-peak (Figure 6) and both comparable peaks of the 5′-d(AGGCG*CCT)$_2$ cross-link. However, since the HX2 proton was coupled to three other protons, namely, its geminal HX1 and both vicinal HX3 protons, the absence of multiplet component peaks meant one of the coupling constants was undetectably small. A plot of the vicinal Karplus correlation depicting the relationship between dihedral angle and $^3J_{HH}$ showed that coupling constants below 0.5 Hz corresponded to dihedral angles in the range 70−95°.[25] A model of diaminopropane was built in Insight II and configured to set the dihedral angle between one HX1 and one HX3 to 90° (Figure 7).

The rest of the structure was manipulated to produce a conformation in which interproton distances between equivalent sets were identical. The result was a helical shape with dihedral angles between vicinal protons of 30°, 90°, and 150°, as shown in Figure 8.

With the dihedral angles of the model available, the vicinal Karplus correlation provided departure points for three-bond coupling constants for each cross-peak. These were used in SPHINX and LINSHA simulations of the respective DQF-COSY cross-peaks (Figure 6). The optimal coupling constants

(25) Silverstein, R. M.; Bassler, G. C.; Morrill, T. C. *Spectrometric Identification of Organic Compounds*, 5th ed.; John Wiley & Sons: New York, 1991.

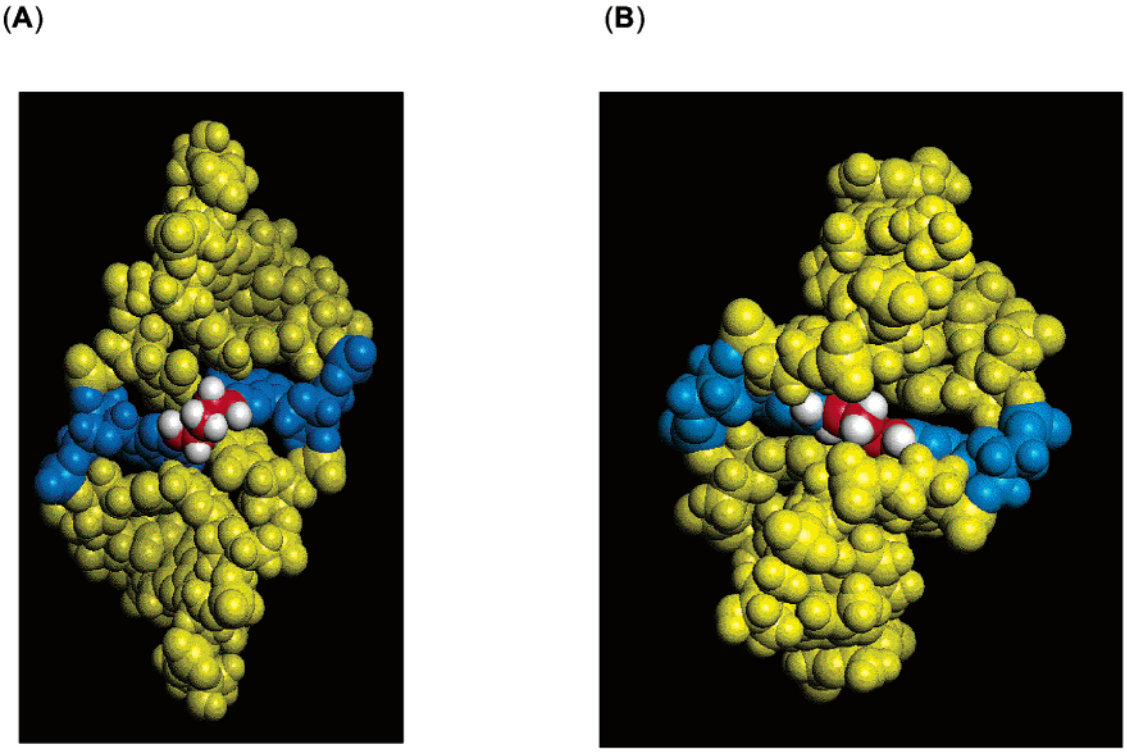

Figure 9. Molecular dynamics-generated structures of (A) −GpC− cross-linked oligomer **2** (5′-d(TCCG*CGGA)$_2$) and (B) −CpG− cross-linked 5′-d(AGGCG*CCT)$_2$ Space-filling representation of the final structure; deoxyguanosine residues tethering the cross-link are in blue, trimethylene carbon atoms, in red.

were 9.5 Hz, corresponding to a dihedral angle of 150°; 6 Hz (30°); and 0.5 Hz (90°). The geminal coupling constant used in the simulation was 13 Hz, which correlated to a three-bond angle of ∼110° according to the geminal Karplus correlation.[25]

The interproton distances of the helical conformation were measured from the resulting model in Insight II and added to the distance restraints used for molecular dynamics calculations described below.

Restrained Molecular Dynamics. Internuclear Distances. A total of 328 experimental intensities, supplemented with calculated intensities from IniA and IniB structures, were used in MARDIGRAS calculations. Distances calculated from poorly resolved, or overlapped intensities, from cross-peaks near the water resonance whose intensities were altered by presaturation of the water signal and from those whose measurements exceeded 5 Å as calculated by MARDIGRAS, were removed if they were inconsistent with a reasonable structure. The final set of 308 interproton distances consisted of 224 intraresidue restraints, including 6 within the trimethylene cross-link, and 84 interresidue restraints (Table S3). An average of 39 intranucleotide, internucleotide, and empirical distances was obtained for each base pair.

The NOE-generated distances along with upper and lower bounds as assigned by MARDIGRAS are shown in the Supporting Information in Table S4. The NOE distance restraints were separated into five quality sets, of which Class 1 contained the 180 best restraints, Class 2 contained 46 restraints, Class 3 contained 30 restraints, Class 4 contained 8 restraints, and Class 5, the 44 worst restraints.

Sugar Torsion Angle Restraints. Values for the dihedral backbone angle δ shown in Table S2 were used to restrain torsion angles during molecular dynamics calculations.

Structural Refinement. The final structures (based on IniA and IniB) were obtained by averaging the ⟨rMD-A⟩ structures and ⟨rMD-B⟩ structures followed by potential energy minimization. The space-filling model of the final averaged structure is shown in Figure 9A; for comparison, the model for the CpG cross-link is shown in Figure 9B.

The rms differences on a per-residue basis between IniA and IniB, resulted in a 4.5 Å rms deviation between the widely divergent conformations of cross-linked A-DNA and B-DNA starting structures. The emergent structure was less dissimilar to A-DNA than to B-DNA, as the rmsd comparison between ⟨rMD$_{av}$⟩ and IniA (3.6 Å) was smaller than the difference between ⟨rMD$_{av}$⟩ and IniB (5.7 Å). The precision of the emergent structures is seen in the convergence to a common structure, whether starting from IniA or IniB, with an average rms deviation of 0.91 Å for the final average structure and a maximum rmsd of 1.2 Å between the two most divergent structures contributing to the average.

Complete Relaxation Matrix Analysis Calculations. The NOE cross-peak intensities measured at a mixing time of 350 ms were compared to intensities derived from relaxation matrix analysis of the refined structures[26] using the sixth-root residual index (R_1x), as shown in Table S5. Consistent results were obtained at each of the three mixing times, with the best values being observed for the 350 ms data. This could be a reflection of the improved sensitivity of the longer mixing time data. The R factor for both IniA and IniB structures at 350 ms was 0.11. In contrast, the R factors of the MD structures which emerged from IniA and IniB were 0.063 and 0.065, respectively.

Structural Analysis. The distortions of the DNA molecule induced by the trimethylene cross-link were quantified using

(26) Keepers, J. W.; James, T. L. *J. Magn. Reson.* **1984**, *57*, 404−426.

DIALS AND WINDOWS.[27] A plate depiction of the emergent $\langle rMD_{av} \rangle$ structure, shown in Figure 10, displays the bend and twist in the helical axis. A comparison of the backbone torsion angles, intra-base-pair parameters, and inter-base-pair parameters for the unmodified and cross-linked oligodeoxynucleotide follows.

Backbone Torsion Angles. The backbone torsion angles $\alpha-\zeta$ were examined graphically (Figure S6 in the Supporting Information) for potential energy-minimized models of the unmodified oligodeoxynucleotide, the trimethylene cross-link, canonical A-DNA, and canonical B-DNA.

Accommodating the trimethylene tether between G*4 and G*12 induced a twist and a bend in the helical axis of the oligomer. The impact on the backbone torsion angles showed a departure from the modeled unmodified oligodeoxynucleotide at internal bases for torsion angles α, β, and ϵ and at 3′-terminal nucleotides for torsion angles β, γ, ϵ, and ζ. The values for δ and ζ torsion angles were more similar to that for the energy-minimized structure, except for the 3′-terminal ζ angle mentioned above. The widely varying torsion angle values from one nucleotide to the next signified that the distortions caused by the cross-link extended beyond the immediate vicinity of the trimethylene tether. In fact, as far away as three residues in either direction the molecule had not recovered its helical shape before the ends began fraying.

Intra-Base-Pair Helical Parameters. Plots of the intra-base-pair parameters calculated from the final structure of unmodified and cross-linked DNA are shown in Figure S7. The parameters of the modeled unmodified oligodeoxynucleotide more closely resembled canonical B-form DNA, but the cross-link exhibited characteristics unlike either canonical A- or B-form DNA.

The twist and bend in the helical axis were quantified in the *y*-displacement and tip parameters. The pattern in *y*-axis displacement, from the cross-link base pairs G*4·C12 and C5·G*13 to the terminal base pairs T1·A16 and A8·T9, paralleled the trend in tip angle for these base pairs. Inclination around the *x*-axis was at its greatest at base pairs G*4·C12 and C5·G*13, as were propeller twist and opening between base pairs. Inclination of base pairs was greatest at the covalently bound G*4·C12 and C5·G*13. However, each base pair buckled to an extent, and the maximum value was observed at C3·G14 and G6·C11, the bases immediately 3′ and 5′ to the trimethylene cross-link.

Inter-Base-Pair Helical Parameters. Inter-base-pair parameters were also examined (Figure S7). Unsurprisingly, base step G*4·C13 to C5·G*12 showed the lowest value for the rise parameter, as the guanines were covalently bound. Accommodating the cross-link at this same base step resulted in the greatest degree of twist, while twist between base steps C2·G15, C3·G14, G7·C10, and G6·C11 was restricted to the lowest value seen in the duplex. The deviation of surrounding base steps from either canonical B-DNA, canonical A-DNA, or the modeled unmodified DNA reinforced the observation that distortions were present as far away as the termini of the strands.

Discussion

Experimental Evidence for the Emergent Structure. The spectroscopic and melting data that distinguished the cross-linked duplex from its unmodified analogue were the most important criteria with which the emergent structure had to conform. Those distinguishing features included the symmetry of the duplex, the upfield shift of the neighboring (and base-pairing) residue C5H1′, missing multiplet component peaks in the vicinal cross-peaks of the cross-link methylene protons in the DQF-COSY, and a complete absence of NOEs between the protons of the trimethylene cross-link and any nonexchangeable protons in the nucleosides.

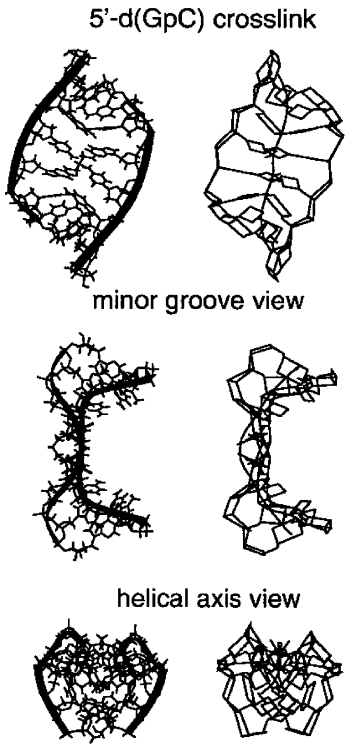

Figure 10. Superposition of the helical axis on the refined rMD structure of cross-linked 5′-d(TCCG*CGGA)$_2$. The bend in the helical axis is evident in both minor groove view and the view from the side of the DNA.

Structure of the Cross-Linked Duplex and Comparison with the CpG Cross-Link. Although the unmodified CpG and GpC duplexes were similar in overall structure, being essentially B-form DNA, there were striking differences between the two cross-linked duplexes as can be seen in the space-filling models shown in Figure 9. In the GpC sequence the conformation of the refined structure resembled neither B- nor A-like DNA. However, continuous interresidue NOE connectivity between anomeric and aromatic protons and base-pairing interactions among the interior six residues observed in the NMR data for the imino protons indicated that the strands were involved in duplex structure. The trimethylene cross-link forced the planes of the purine bases of the attached deoxyguanosines to be rotated away from each other, that is, toward the 5′ ends of each respective strand. Additionally, the deoxycytosines with which the guanines were base-paired suffered twisting distortion that appeared to prevent base-stacking between these residues. In contrast, in the CpG structure the guanines involved in the cross-link remain essentially planar, allowing continued base-stacking and stabilization of the duplex.

Configuration of the Residues Near the Cross-Link. In DNA duplexes containing the monoadducts of mitomycin[28]

(27) Ravishankar, G.; Swaminathan, S.; Beveridge, D. L.; Lavery, R.; Sklenar, H. *J. Biomol. Struct. Dyn.* **1989**, *6*, 669−699.

styrene oxide,[29] anthramycin[30] and stereoisomers of benzo[*a*]-pyrene diol epoxide,[31−34] the substituent replaces the exo proton, that is, the one closest to N3, leaving the endo proton available to participate in Watson−Crick hydrogen bonding. Guanine N^2-to-N^2 cross-linked adducts of mitomycin C[35] and a distamycin−pyrrole conjugate[36] also replace the exo proton. Except for the benzo[*a*]pyrene adducts, the solution structures of the above-listed DNA adducts contain a torsion angle defined by the atoms guanine N1−C2−N^2-(adduct attachment carbon atom) close to 180°. This angle for four stereoisomers of *anti*-benzopyrenyl adducts ranges from 135° to 152°.[37] For the present study, models of suitable starting structures for the trimethylene cross-link in which the exo proton had been replaced by a methylene carbon were built in both canonical A-DNA and canonical B-DNA. Restrained molecular dynamics structures that were generated with these starting structures contained features disallowed by the experimental data. For example, the trimethylene cross-link protons were well within NOE-observable distance of each other in the emergent structure, but the experimental data could not account for any such interaction. Only with the substitution of the endo proton were structures obtained which agreed with the experimental evidence. This was also the case with the CpG cross-link.

Conformation of the Trimethylene Cross-Link Tether. The symmetry of the tether and the missing DQF-COSY multiplet splitting signals between methylene protons of the tether pointed to a helical conformation for the tether in the GpC cross-link. Were it not for the driving force of the guanine exocyclic amino group retaining planarity with the purine ring, other conformations of the tether might have been accommodated. In contrast, on the basis of a similar analysis of the DQF-COSY spectra of the trimethylene protons, it appears that the tether in the CpG cross-link adopts a planar W conformation.

Helical Distortion of the Cross-Link. For the GpC cross-link, the NMR studies indicate that the helical axis of the DNA is both bent and twisted in the vicinity of the cross-link and that the major and minor grooves appear to be flat at the GpC segment (Figure 10). However, bending studies using a gel retardation assay with oligomers of a 21-mer containing the 8-mer sequence failed to show significant bending. While we cannot rule out a fortuitous 180° phasing of the bends, it seems more likely that the bend observed in the 8-mer is an artifact resulting from the oligonucleotide being so short. The CpG cross-link did not show any detectable bending in the gel mobility assay.

In the case of the GpC cross-link, the lower melting temperature (compared to that of the unmodified duplex) as determined by UV spectroscopy and the even lower temperature at which the imino protons underwent exchange with water support gross distortions and destabilization of the overall structure of the oligonucleotide duplex. These observations raise questions concerning the reliability of the structure determined in this study. The sharpness and symmetry of the ^{1}H spectrum militate against a mixture of slowly equilibrating structures, but rapidly equilibrating species is an undeniable possibility. The spectra were obtained well below the T_m (25 versus 52 °C). Nevertheless, Figure 1B shows that the penultimate hydrogen bonds are frayed even at 25 °C and that the hydrogen bonds involving the cross-linked G's are still intact. Although 21-mer duplex **3** did not show the bending seen in the 8-mer duplex, it also showed partial melting several degrees below the T_m of unmodified 21-mer duplex, indicating that even in a much longer sequence the GpC cross-link is destabilizing. In contrast to these results, the cross-linked CpG 8-mer duplex did not show significant melting even at 80 °C (T_m = 60 °C for uncross-linked 5′-d(AGGCGCCT)$_2$), indicating a high degree of stabilization introduced by the cross-link. Thus, although the structure determined in the present study shows more distortion than would be present in a longer piece of DNA, the basic conclusion remains that DNA containing the GpC cross-link is thermodynamically less stable than that containing the CpG cross-link.

Possible Structures of the Malondialdehyde Cross-Link. The linkage in MDA-cross-linked duplexes is believed to be between the exocyclic amino groups of guanines.[9] Possible structures include one with two imines, Pu−N═CH−CH_2−CH═N−Pu, or with one imine and one enamine, Pu−N═CH−CH═CHNH−Pu (Scheme 1). In both cases, two of the bonds in the tether are double bonds requiring the atoms of the double bond and of the substituents on the double bond to lie in a plane. This constraint is easily met by the previously determined structure of the trimethylene cross-link in the CpG sequence because the carbon and nitrogen atoms of the tether and the two purine rings lie almost in a single plane. However, in the GpC sequence the purine rings lie in separate planes, and the trimethylene tether between them adopts a helical conformation creating torsional angles of 145° for Pu−N−C−C and 88° for N−C−C−C. Consequently, neither the imine nor the enamine structure can be built by simply changing the hybridization of atoms in the tether. For an MDA cross-link to be formed in the GpC sequence, the duplex would have to adopt some other conformation. In that the duplex containing the trimethylene cross-link in the GpC sequence is already thermodynamically less stable than in the reverse sequence, it is probable that the MDA cross-link would also be thermodynamically less stable in a GpC duplex, that is, less likely to be formed in a significant amount, than in a CpG sequence. There is also a kinetic factor favoring the CpG cross-link; comparison of the structures of the unmodified duplexes shows that the exocyclic amino groups of the reacting guanines are closer in the CpG sequence (3.56 versus 4.82 Å) with better juxtaposition of the bases. One or both of the MDA−guanine linkages might be in the carbinolamine form rather than imine or enamine. Even then, the CpG

(28) Sastry, M.; Fiala, R.; Lipman, R.; Tomasz, M.; Patel, D. J. *J. Mol. Biol.* **1995**, *247*, 338−359.
(29) Zegar, I. S.; Setayesh, F. R.; DeCorte, B. L.; Harris, C. M.; Harris, T. M.; Stone, M. P. *Biochemistry* **1996**, *35*, 4334−4348.
(30) (a) Krugh, T. R.; Graves, D. E.; Stone, M. P. *Biochemistry* **1989**, *28*, 9988−9994. (b) Boyd, F. L.; Cheatham, S. F.; Remers, W.; Hill, G. C.; Hurley, L. H. *J. Am. Chem. Soc.* **1990**, *112*, 3279−3289.
(31) Cosman, M.; De Los Santos, C.; Fiala, R.; Hingerty, B. E.; Singh, S. B.; Ibanez, V.; Margulis, L. A.; Live, D.; Geacintov, N. E.; Broyde, S.; Patel, D. J. *Proc. Natl. Acad. Sci. U.S.A.* **1992**, *89*, 1914−1918.
(32) de los Santos, C.; Cosman, M.; Hingerty, B. E.; Ibanez, V.; Margulis, L. A.; Geacintov, N. E.; Broyde, S.; Patel, D. J. *Biochemistry* **1992**, *31*, 5245−5252.
(33) Cosman, M.; de los Santos, C.; Fiala, R.; Hingerty, B. E.; Ibanez, V.; Luna, E.; Harvey, R.; Geacintov, N. E.; Broyde, S.; Patel, D. J. *Biochemistry* **1993**, *32*, 4145−4155.
(34) Cosman, M.; Hingerty, B. E.; Luneva, N.; Amin, S.; Geacintov, N. E.; Broyde, S. *Biochemistry* **1996**, *35*, 9850−9863.
(35) Norman, D.; Live, D.; Sastry, M.; Lipman, R.; Hingerty, B. E.; Tomasz, M.; Broyde, S.; Patel, D. J. *Biochemistry* **1990**, *29*, 2861−2875.
(36) Fagan, P. A.; Spielmann, H. P.; Sigurdsson, S.; Rink, S. M.; Hopkins, P. B.; Wemmer, D. E. *Nucleic Acids Res.* **1996**, *8*, 1566−1573.
(37) Geacintov, N. E.; Cosman, M.; Hingerty, B. E.; Amin, S.; Broyde, S.; Patel, D. J. *Chem. Res. Toxicol.* **1997**, *10*, 111−146.

Scheme 3

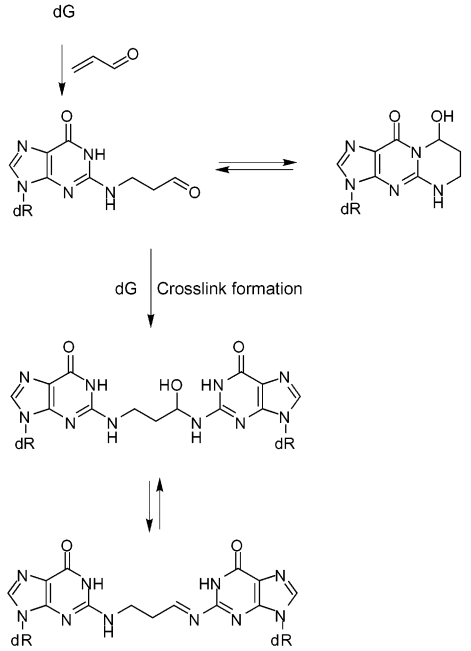

cross-link would form to the exclusion of the GpC for the reasons stated below with respect to acrolein cross-links.

Possible Structures of the Acrolein Cross-Link. The arguments in the preceding section apply equally strongly to the recently described DNA interstrand cross-links of acrolein.[38,39] Treatment of dG with acrolein under physiological conditions leads to γ-hydroxy-1,N^2-propano-dG (the nucleoside of 8-hydroxy-5,6,7,8-tetrahydropyrimido[1,2-*a*]purin-10(3*H*)-one).[40] This adduct is formed by conjugate addition of N^2 to the double bond of acrolein to give N^2-(3-oxopropyl)-dG followed by ring closure involving attack of N1 on the aldehyde. In ds DNA, the cyclic adduct opens to regenerate N^2-(3-oxopropyl)-dG,[41] which in the 5′-(CpG) sequence reacts with the exocyclic amino group of the guanine in the opposite chain (Scheme 3), forming a carbinolamine cross-link which has been detected by $^{15}N-^{1}H$ HSQC NMR experiments using an ^{15}N label in the exocyclic amino group of the target guanine in the complementary strand.[38] The carbinolamine is in equilibrium with imine. Probably the equilibrium favors the carbinolamine; however, sufficient imine is present that it can be trapped by reduction with $NaCNBH_3$.

The interchain cross-linking reaction is strongly dependent on sequence; no indication for formation of carbinolamine- or imine-type cross-links could be obtained for the acrolein adduct in a GpC sequence context. The failure to form imine, as evidenced by inability to trap the imine by reduction, is readily accounted for by nonplanarity of the tether in the 8-mer duplex described in this work. However, as discussed in the accompanying contribution,[39] the interchain carbinolamine cross-link, if formed at all, is also below the level of detection in an HSQC experiment. The explanation for this lies in the fact that the formation of carbinolamine (and imine) is a reversible process. T_m studies have shown the trimethylene cross-link strongly stabilizes duplex structure in the CpG sequence context, whereas the present T_m study shows the cross-link is destabilizing in GpC. Thus, formation of the carbinolamine cross-link is thermodynamically favored in the CpG sequence but disfavored in the GpC.

Effect of Sequence Context on Structures of Cross-Links between Exocyclic Amino Groups of Cytosines. Interesting and related observations of the influence of sequence context on the stability of interstrand cross-links was recently reported by Miller for oligonucleotides containing alkyl tethers between N^4 positions of cytosine in CpG and GpC sequence contexts.[42] Although their studies employed a two-carbon linker rather than the three-carbon linker studied in our laboratory, the sequence effects observed for the cytosine cross-links were similar to those found in our studies, that is, in the CpG sequence the cross-link greatly stabilized the duplex, whereas in the GpC sequence the cross-link was destabilizing. Neither the minor groove N^2-N^2 dG three-carbon cross-link nor the major groove N^4-N^4 dC two-carbon cross-link appeared to induce significant bending in the CpG sequence. The bending induced by the N^4-N^4 cross-link in the GpC context could not be evaluated because the self-ligation of the 10-mer failed. In our case the self-ligation probably succeeded because the oligonucleotide used for the bending studies was a 21-mer (**3**). Although the NMR studies of the 8-mer indicated bending of the helix in the region of the cross-link, no bending was detected in the gel mobility studies of the longer oligonucleotide.

Summary

The structures of duplexes cross-linked by a trimethylene tether between the exocyclic amino groups of guanines in opposing strands have been examined in two sequence contexts, CpG and GpC, in an effort to understand the strong preference of agents such as malondialdehyde and acrolein to form detectable cross-links only in the CpG context. The cross-link in the CpG sequence was found to assume an almost planar conformation and to stabilize the duplex, whereas the GpC cross-link adopted a helical conformation and destabilized the duplex. Although both cross-link conformations could accommodate a carbinolamine intermediate, only the CpG sequence would be amenable to formation of a planar imine or enamine. Since the reactions involved in these cross-links are readily reversible, the thermodynamic instability introduced into the duplex by the cross-link in the GpC sequence would account for the sequence preference.

Accession Codes. The coordinates of the lowest-energy structure have been deposited in the PDB (accession codes: RCSB ID is RCSB016282; PDB ID is 1LUH) together with the restraints used in the structure calculation.

Acknowledgment. We gratefully acknowledge support of this research by the National Institute for Environmental Health Sciences (Grants ES07781 and ES00267). Funding for the NMR spectrometer was supplied by a grant from the NIH shared instrumentation program, (Grant RR05805) and the Vanderbilt Center in Molecular Toxicology (Grant ES00267). We thank Mr. Markus Voehler for valuable assistance with NMR spectroscopy.

(38) Kim, H.-Y. H.; Voehler, M.; Harris, T. M.; Stone, M. P. *J. Am. Chem. Soc.* **2002**, *124*, 9324−9325.
(39) Kozekov, I. D.; Nechev, L. V.; Moseley, M. S.; Harris, C. M.; Rizzo, C. J.; Stone, M. P.; Harris, T. M. *J. Am. Chem. Soc.* **2002**, *124*, 50−61.
(40) Chung, F. L.; Hecht, S. S.; Palladino, G. *IARC Sci. Publ.* **1986**, *70*, 207−25.
(41) de los Santos, C.; Zaliznyak, T.; Johnson, F. *J. Biol. Chem.* **2001**, *276*, 9077−9082.
(42) Noronha, A. M.; Noll, D. M.; Wilds, C. J.; Miller, P. S. *Biochemistry* **2002**, *41*, 760−771.

Supporting Information Available: Experimental details of synthesis of the cross-linked duplexes **2** and **3**, for the acquisition and analysis of NMR spectra, and for the measurement of DNA bending and melting, Table S1 (selected chemical shifts in adducted oligonucleotide **2**), Table S2 (deoxyribose ring dihedral torsion angles for **2**), Table S3 (distribution of experimental restraints among nucleotide units of **2**), Table S4 (distance restraints from NOE data), Table S5 (comparison of sixth root residual indices R_1x), Figure S1 (^{1}H spectrum of cross-linked oligonucleotide), Figure S2 (expanded plot of a phase-sensitive NOESY spectrum), Figure S3 (regions of the 10 °C water NOESY), Figure S4 (evolution of the restrained molecular dynamics average structure), Figure S5 (per residue comparisons between initial structures and final structures for the cross-linked oligodeoxynucleotide), Figure S6 (helicoidal analysis (backbone torsion angles ($\alpha-\zeta$), glycosidic torsion angles (χ), and sugar pseudorotation angles (ϕ)), Figure S7 (helicoidal analysis (intra-base-pair and inter-base-pair parameters for the *r*MD structures of the unmodified and cross-linked oligodeoxynucleotide)), Figure S8 (electrophoresis gel of ligation ladders and graphical analysis of the bending study) (PDF). This material is available free of charge via the Internet at http://pubs.acs.org.

JA0207798